metry elements of a bicrystal. The former must always be perpendicular to the interfacial plane and the later parallel to it (except of colour-reversing rotoinversion axes; see § 2). In order to take into account these restrictions, we consider that the symmetry group of the dichromatic complex is sectioned by a unique two-sided plane. Thus, the symmetry of the bicrystal associated with the particular orientation of the interfacial plane is expressed by the set of symmetry operations of the dichromatic group that leave the two-sided sectional plane invariant. This procedure provides us with a comprehensive method for investigating generic relations amongst bicrystals corresponding to the same misorientation relationship of their components.

The most important conclusion achieved by studying the bicrystal symmetry by this method is that crystallographically equivalent interfacial planes create bicrystals with symmetry-related structures. Symmetry-related bicrystals arise as a consequence of dissymmetrization, and in this respect the idea of regarding a bicrystal as having been created by sectioning the corresponding dichromatic complex is most helpful.

Further examination of generic relations amongst bicrystals can be accomplished by employing the proposed classification of interfaces. The distinction of four types of interfaces, namely completely rigid, orientation-rigid, elevation-rigid and non-rigid interfaces, is important in connection with the physical properties of bicrystals. For the first three types of interfaces a small deviation from the orientation and/or position of the corresponding interfacial plane may be related to a sharp transition in the properties of the bicrystals. On the other hand, the symmetry considerations presented in this paper indicate that non-rigid interfaces can exhibit smooth changes of their physical properties over a wide range of interfacial orientations.

References

AIZU, K. (1970). *Phys. Rev. B*, **2**, 754-772.

POND, R. C. (1977). *Proc. R. Soc. London Ser. A*, **357**, 471-483.

POND, R. C. & BOLLMANN, W. (1979). *Philos. Trans. R. Soc. London*, **292**, 449-472.

POND, R. C. & VLACHAVAS, D. S. (1983). *Proc. R. Soc. London Ser. A*, **386**, 95-143.

TENDELOO, G. VAN & AMELINCKX, S. (1974). *Acta Cryst.* A**30**, 431-440.

VLACHAVAS, D. S. (1980). *Symmetry and Structure of Bicrystals.* PhD thesis, Univ. of Liverpool.

VLACHAVAS, D. S. (1984*a*). *Acta Cryst.* A**40**, 200-213.

VLACHAVAS, D. S. (1984*b*). *Acta Cryst.* A**40**, 213-221.

Acta Cryst. (1985). A**41**, 376-382

Pseudo-Weak-Phase-Object Approximation in High-Resolution Electron Microscopy. I. Theory

BY F. H. LI AND D. TANG

Institute of Physics, Academia Sinica, Beijing, China

(*Received* 14 *May* 1984; *accepted* 24 *January* 1985)

Abstract

On the basis of the dynamical electron diffraction theory of Cowley & Moodie [*Acta Cryst.* (1957), **10**, 609-619], a new formula has been derived for the multiple-beam image intensity expressed in terms of the projected potential distribution as well as the specimen thickness. According to this formula, crystals for which the weak-phase-object approximation does not hold can be treated by the pseudo-weak-phase-object approximation (PWPOA) up to a certain critical thickness. Here the real crystal is replaced by its imaginary isomorph, where the constituent heavy atoms behave as lighter atoms than those of the real crystal, and *vice versa*. The validity of the PWPOA is discussed and confirmed by the comparison of the images of chlorinated Cu phthalocyanine calculated with PWPOA and the multislice method.

1. Introduction

According to the weak-phase-object approximation (WPOA) the image intensity is expressed as

$$I(x, y) = 1 - 2\sigma\varphi(x, y) \qquad (1.1)$$

under the optimum defocus condition (Scherzer, 1949; Cowley & Iijima, 1977), where $\sigma = \pi/\lambda E$, λ is the wavelength of electrons, E the accelerating voltage and $\varphi(x, y)$ the projection of the potential distribution function (PPDF) of the weak phase object along the beam direction. Formula (1.1) shows a linear relationship between the image intensity and the PPDF. But it is well known that structure images corresponding to the projection of the crystal structure can be obtained with specimens considerably thicker than the WPOA holds for. This was inter-

0108-7673/85/040376-07$01.50

preted by a simple theory of large phase changes (Cowley & Iijima, 1972) and the projected charge density approximation (Cowley & Moodie, 1960; Allpress, Hewat, Moodie & Sanders, 1972; Lynch & Moodie, 1975). Nevertheless, for direct observation of the crystal structure or defect by high-resolution electron microscopy it is still desirable to prepare the specimens as thin as possible, because for too thick crystals the dynamical scattering may cause drastic deviation of the image from the projection of the crystal structure even if the image is taken under the optimum defocus condition (Grinton & Cowley, 1971; Cowley & Iijima, 1977; Ishizuka & Iijima, 1981; Uyeda, Kobayashi, Ishizuka & Fujiyoshi, 1978–79; Kirkland, Siegel, Uyeda & Fujiyoshi, 1980; Li & Hashimoto, 1984).

However, on the other hand the dynamical scattering effect is useful for enhancing the image contrast of light atoms when the crystal consists of heavy and light atoms. In addition, there is an optimum crystal thickness, which is most advantageous for revealing the light atoms together with the heavy atoms in the image with sufficient contrast (Li & Hashimoto, 1984).

In the present paper the dependence of the image intensity on the PPDF as well as the thickness of the sample has been studied.

2. Approximation to the multiple-beam dynamical electron diffraction theory

According to the multiple-beam dynamical diffraction theory formulated by Cowley & Moodie (1957), transmission of electrons through a sample is represented by transmission through each slice and propagation of electrons from one slice to the next.

If the examined crystal can be divided into the same slices of very small thickness, for instance about 3 Å, then each slice will act as a weak phase object. If the absorption is ignored, the transmission function of one slice can be expressed as

$$q_1(x, y) = 1 - i\sigma\varphi(x, y) \tag{2.1}$$

for an incident plane wave with unit amplitude, where $\varphi(x, y)$ is the PPDF for one slice.

The phase shift of the electron wave passing through each slice is assumed to take place at the bottom. The wave transmitted through the first slice and subsequently propagated to the bottom of the second slice is expressed as

$$q_1(x, y) * p(x, y) = 1 - i\sigma\varphi(x, y) * p(x, y). \tag{2.2}$$

Here $*$ represents the operation of convolution and $p(x, y)$ the Fresnel propagation function:

$$p(x, y) = (i/t)\exp[-(i\pi/t)(x^2+y^2)], \tag{2.3}$$

where

$$t = \lambda\Delta z \tag{2.4}$$

and Δz is the slice thickness. The wave function of electrons leaving the second slice is

$$\begin{aligned} q_2(x, y) &= q_1(x, y)[q_1(x, y) * p(x, y)] \\ &= 1 - i\sigma\varphi(x, y) - i\sigma\varphi(x, y) * p(x, y) \\ &\quad - \sigma^2\varphi(x, y)[\varphi(x, y) * p(x, y)]. \end{aligned} \tag{2.5}$$

The last term on the right-hand side of (2.5) indicates the double scattering, which can be ignored compared with the first-order term of $\varphi(x, y)$ for very thin slices. Hence,

$$q_2(x, y) = 1 - i\sigma\varphi(x, y) - i\sigma\varphi(x, y) * p(x, y). \tag{2.6}$$

Obviously, $q_2(x, y)$ is just the transmission function of the crystal consisting of two slices.

Let $q_{n+1}(x, y)$ represent the transmission function of the crystal consisting of $n+1$ slices, then

$$\begin{aligned} q_{n+1}(x, y) = q_1(x, y)_n(\cdots{}_2\{q_1(x, y) \\ \times{}_1[q_1(x, y) * p(x, y)]_1 \\ * p(x, y)\}_2 * \cdots * p(x, y))_n. \end{aligned} \tag{2.7}$$

If the multiple scattering is ignored in each slice, $q_{n+1}(x, y)$ can be simplified as

$$\begin{aligned} q_{n+1}(x, y) \\ &= 1 - i\sigma\varphi(x, y) - i\sigma\varphi(x, y) * p(x, y) \\ &\quad - i\sigma\varphi(x, y) * p(x, y) * p(x, y) \ldots \\ &\quad - i\sigma\varphi(x, y) * \underbrace{p(x, y) * p(x, y) * \ldots * p(x, y)}_{* \; n \text{ times}}. \end{aligned} \tag{2.8}$$

The Fourier transform of (2.8) gives the diffracted wave function at the back focal plane of the objective lens for the crystal consisting of $n+1$ slices:

$$\begin{aligned} Q_{n+1}(u, v) &= \delta(u, v) - i\sigma F(u, v) \\ &\quad - i\sigma F(u, v)\sum_{j=1}^{n} P^j(u, v), \end{aligned} \tag{2.9}$$

where $\delta(u, v)$ denotes the Dirac delta function and

$$F(u, v) = \mathcal{F}[\varphi(x, y)], \tag{2.10}$$

$$P(u, v) = \mathcal{F}[p(x, y)]. \tag{2.11}$$

$\mathcal{F}$ is the symbol of Fourier transform operation. $F(u, v)$ is the kinematical structure factor. The Fourier transform of (2.3) yields

$$P(u, v) = \exp[i\pi t(u^2+v^2)], \tag{2.12}$$

then

$$P^j(u, v) = \exp[i\pi jt(u^2+v^2)]. \tag{2.13}$$

3. Multiple-beam image intensity

It is well known that the defocus and the spherical aberration of the lens introduce a phase factor $\exp[i\chi(u, v)]$ to the electron waves in the back focal plane of the lens. Here

$$\chi(u, v) = \pi C_s \lambda^3 (u^2+v^2)^2/2 + \pi \Delta f \lambda (u^2+v^2), \quad (3.1)$$

where C_s represents the spherical aberration coefficient and Δf the defocus amount (positive for overfocus). Since under the optimum defocus condition the imaginary part of the phase factor, $\sin\chi$, is roughly equal to -1 in a considerably wide range of the spatial frequency and the real part $\cos\chi$ is negligibly small (Scherzer, 1949),

$$\exp[i\chi(u, v)] = -i. \quad (3.2)$$

Hence, under the optimum defocus condition the modified diffracted wave function for the crystal consisting of $n+1$ slices is

$$Q_{n+1}(u, v)\exp[i\chi(u, v)] = \delta(u, v) - \sigma F(u, v) - \sigma F(u, v)\sum_{j=1}^{n} P^j(u, v). \quad (3.3)$$

The Fourier transform of (2.16) gives the wave function on the image plane for the crystal consisting of $n+1$ slices as

$$\psi_{n+1}(x, y) = 1 - \sigma\varphi(x, y) - \sigma\varphi(x, y) * \sum_{j=1}^{n} \mathcal{F}^{-1}[P^j(u, v)]. \quad (3.4)$$

Because

$$\mathcal{F}^{-1}[P^j(u, v)] = \iint \exp[i\pi jt(u^2+v^2)] \times \exp[-2\pi i(xu+yv)]\,du\,dv = (1/jt)\sin(\pi/jt)(x^2+y^2) + (i/jt)\cos(\pi/jt)(x^2+y^2), \quad (3.5)$$

(3.4) can be expressed as

$$\psi_{n+1}(x, y) = 1 - \sigma\varphi(x, y) - \sigma\varphi(x, y) * \sum_{j=1}^{n} S_j(x, y) - i\sigma\varphi(x, y) * \sum_{j=1}^{n} C_j(x, y), \quad (3.6)$$

where

$$S_j(x, y) = (1/jt)\sin(\pi/jt)(x^2+y^2), \quad (3.7)$$

$$C_j(x, y) = (1/jt)\cos(\pi/jt)(x^2+y^2). \quad (3.8)$$

Hereafter $S_j(x, y)$ will be called a Fresnel sine function and $C_j(x, y)$ a Fresnel cosine function of order j.

Hence, the image intensity for the crystal consisting of $n+1$ slices is

$$\begin{aligned} I_{n+1}(x, y) &= |\psi_{n+1}(x, y)|^2 \\ &= \left[1 - \sigma\varphi(x, y) - \sigma\varphi(x, y) * \sum_{j=1}^{n} S_j(x, y)\right]^2 + \left[\sigma\varphi(x, y) * \sum_{j=1}^{n} C_j(x, y)\right]^2 \\ &= 1 - 2\sigma\varphi(x, y) + \sigma^2\varphi^2(x, y) - 2\sigma\varphi(x, y) * \sum_{j=1}^{n} S_j(x, y) \\ &\quad + 2\sigma^2\varphi(x, y)\left[\varphi(x, y) * \sum_{j=1}^{n} S_j(x, y)\right] + \sigma^2\left[\varphi(x, y) * \sum_{j=1}^{n} S_j(x, y)\right]^2 \\ &\quad + \sigma^2\left[\varphi(x, y) * \sum_{j=1}^{n} C_j(x, y)\right]^2. \end{aligned} \quad (3.9)$$

The first two terms in the final expressions for $I_{n+1}(x, y)$ represent the image intensity for the one-slice crystal, or rather the image intensity in WPOA. $\sigma^2\varphi^2(x, y)$ can be ignored as usual, compared with $2\sigma\varphi(x, y)$ while all other additional terms in (3.9) are significant because they are dependent upon the crystal thickness and modify the image contrast appreciably with increase in thickness. Note that the first-order terms of $\varphi(x, y)$ would increase the image contrast with the crystal thickness while the second-order terms decrease it.

4. Fresnel sine and cosine spread PPDF

In order to evaluate the overall influence of all additional terms in equation (3.9), the convolutions of the PPDF $\varphi(x, y)$ with the Fresnel sine and cosine functions are analysed. For simplicity, a Gaussian function

$$G(r) = A\exp(-r^2/R^2) \quad (4.1)$$

is used instead of $\varphi(x, y)$, where

$$r^2 = x^2 + y^2. \quad (4.2)$$

In the radial coordinate system the Fresnel sine and cosine functions given in (3.7) and (3.8) are written as

$$S_j(r) = (1/jt)\sin(\pi/jt)r^2 \quad (4.3)$$

and

$$C_j(r) = (1/jt)\cos(\pi/jt)r^2. \quad (4.4)$$

The convolution of $G(r)$ with $S_j(r)$ yields

$$G(r) * S_j(r) = [A\pi R^2/(j^2t^2+\pi^2R^4)] \times\{\pi R^2 \cos[\pi jtr^2/(j^2t^2+\pi^2R^4)] + jt \sin[\pi jtr^2/(j^2t^2+\pi^2R^4)]\} \times \exp[-r^2/(R^2+j^2t^2/\pi^2R^2)]. \quad (4.5)$$

The convolution of $G(r)$ with $C_j(r)$ yields

$$G(r) * C_j(r) = A\pi R^2/(j^2t^2+\pi^2R^4) \times\{jt \cos[\pi jtr^2/(j^2t^2+\pi^2R^4)] - \pi R^2 \sin[\pi jtr^2/(j^2t^2+\pi^2R^4)]\} \times \exp[-r^2/(R^2+j^2t^2/\pi^2R^2)]. \quad (4.6)$$

Equations (4.5) and (4.6) show that the convolution of a Gaussian function with either a Fresnel sine or a Fresnel cosine function results in another Gaussian function:

$$G'(r) \propto \exp[-r^2/(R^2+j^2t^2/\pi^2R^2)]. \quad (4.7)$$

The standard deviation of $G'(r)$ is greater than that of the original Gaussian function and increases monotonically with the increase of j. This means that the greater j is the wider $G'(r)$ spreads.

Figs. 1(a), (b) and (c) illustrate the forms of the Fresnel sine function, the Gaussian function (4.1) and their convolution for $j=1$, 15 and 30 respectively. Fig. 2 shows the same for the case of the Fresnel cosine functions. Here $R=0{\cdot}5$ Å, $A=1$ and $t=0{\cdot}0526$ Å^2. The variations of

$$G(r) * S_j(r)|_{r=0} = A\pi^2R^4/(j^2t^2+\pi^2R^4) \quad (4.8)$$

and of

$$G(r) * C_j(r)|_{r=0} = A\pi R^2jt/(j^2t^2+\pi^2R^4) \quad (4.9)$$

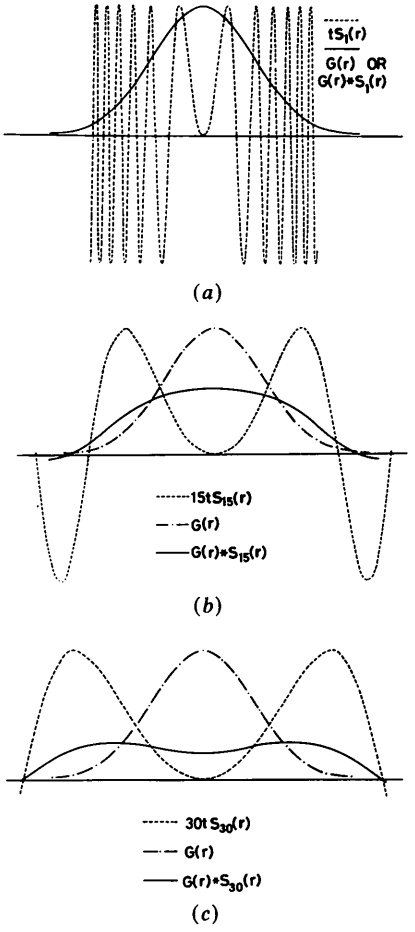

Fig. 1. Curves of the Fresnel sine function multiplied by jt, $jtS_j(r)$, function $G(r)$ and the convolution $G(r) * S_j(r)$ for (a) $j=1$, (b) $j=15$ and (c) $j=30$. The curve of $G(r) * S_1(r)$ and that of $G(r)$ almost coincide for small r as shown in (a). Here $A=1$, $R=0{\cdot}5$ Å, $t=0{\cdot}0526$ Å^2.

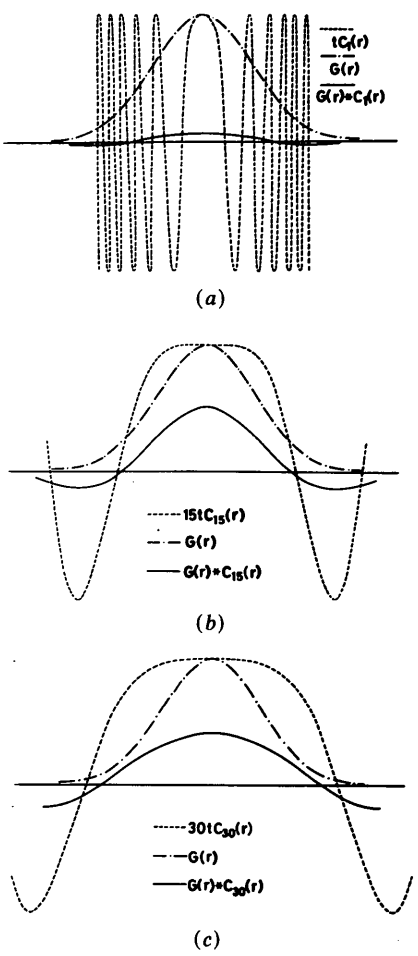

Fig. 2. Curves of the Fresnel cosine function multiplied by jt, $jtC_j(r)$, function $G(r)$ and the convolution $G(r) * C_j(r)$ for (a) $j=1$, (b) $j=15$ and (c) $j=30$. Here $A=1$, $R=0{\cdot}5$ Å, $t=0{\cdot}0526$ Å^2.

with the value of j are very different to each other as shown in Fig. 3. When $j < R^2/t$,

$$G(r) * S_j(r)|_{r=0} > G(r) * C_j(r)|_{r=0},$$

and *vice versa.*

It is expected that the convolution of a real PPDF $\varphi(x, y)$ with the Fresnel sine and cosine functions would act as in the case of a Gaussian function: the convolution of $\varphi(x, y)$ with $S_j(x, y)$ and $C_j(x, y)$ would result in a function spread wider than $\varphi(x, y)$. Therefore, $\varphi(x, y) * S_j(x, y)$ and $\varphi(x, y) * C_j(x, y)$ are recognized as Fresnel-sine- and Fresnel-cosine-spread PPDFs respectively. Furthermore, there should be a certain value j_c, for which when $j < j_c$ the Fresnel sine spread PPFD would have a greater value than the Fresnel cosine spread PPDF at the positions of the atoms, and *vice versa.*

5. Pseudo-weak-phase-object approximation

If $\sigma^2\varphi^2(x, y)$ is ignored, (3.9) can be rewritten as

$$I_{n+1}(x, y) = 1 - 2\sigma\varphi_{n+1}(x, y), \tag{5.1}$$

where

$$\varphi_{n+1}2(x, y) = \varphi(x, y) + \Delta\varphi_{n+1}(x, y) \tag{5.2}$$

and

$$\begin{aligned}\Delta\varphi_{n+1}(x, y) = {} & \varphi(x, y) * \sum_{j=1}^{n} S_j(x, y) \\ & - \sigma\varphi(x, y)[\varphi(x, y) * \sum_{j=1}^{n} S_j(x, y)] \\ & - \frac{\sigma}{2}\left[\varphi(x, y) * \sum_{j=1}^{n} S_j(x, y)\right]^2 \\ & - \frac{\sigma}{2}\left[\varphi(x, y) * \sum_{j=1}^{n} C_j(x, y)\right]^2. \end{aligned} \tag{5.3}$$

Owing to the formal resemblance of (5.1) to the expression for WPOA it is reasonable to treat $\varphi_{n+1}(x, y)$ as the PPDF of a pseudo weak phase object.

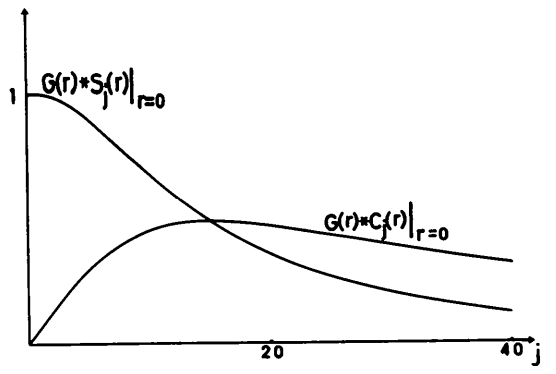

Fig. 3. Dependence of $G(r) * S_j(r)|_{r=0}$ and $G(r) * C_j(r)|_{r=0}$ upon the slice number j. $A = 1$, $R = 0{\cdot}5$ Å, $t = 0{\cdot}0526$ Å

The increment $\Delta\varphi_{n+1}(x, y)$ is closely related to the crystal thickness or the slice number n. The first-order terms of $\varphi(x, y)$ given on the right-hand side of (5.3) introduce a positive increment while all second-order terms introduce a negative one. On the basis of the knowledge about the Fresnel sine and Fresnel cosine spread PPDF it is easy to imagine that $\varphi_{n+1}(x, y)$ would spread wider and wider with the increase in n. In addition, for very small n the peak height of a Fresnel-sine-spread PPDF is much greater than that of the corresponding cosine one, so that the positive terms in (5.3) play an essential role while the sum of all negative terms is negligible. This leads to an approximately linear relationship between $\varphi(x, y)$ and the increment $\Delta\varphi_{n+1}(x, y)$. Thus, $\Delta\varphi_{n+1}(x, y)$ and $\varphi_{n+1}(x, y)$ would have their peaks at the same positions as $\varphi(x, y)$ and peak heights almost linearly related to those of $\varphi(x, y)$. With the increase of n, the Fresnel-cosine-spread PPDF terms in (5.3) become non-negligible and the relationship between $\varphi_{n+1}(x, y)$ and $\varphi(x, y)$ begins to deviate from the linear one. But for ordinary n, $\varphi_{n+1}(x, y)$ may still have its peaks at the same position as $\varphi(x, y)$ and the peak heights monotonically relate to those of $\varphi(x, y)$. When n reaches a critical value n_c, $\varphi_{n+1}(x, y)$ would be equal to zero at the position of the heaviest atoms. With further increase of n, $\varphi_{n+1}(x, y)$ would have negative peaks at the positions of the relatively heavier atoms and positive peaks at the positions of the lighter atoms so that $\varphi_{n+1}(x, y)$ would no more resemble $\varphi(x, y)$. This is schematically shown in Fig. 4.

Hence, if the crystal is thick for the WPOA to hold but thinner than the critical thickness ($n_c\Delta z$), which

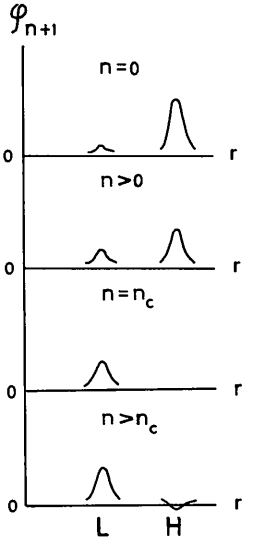

Fig. 4. Variation of function $\varphi_{n+1}(x, y)$ with the slice number n. n_c denotes the critical slice number, L the position of the light atom and H the position of the heavy atom. When $n = n_c$, $\varphi_{n+1}(x, y)$ becomes zero at the positions of the heavy atoms.

depends upon the heaviest atom in the crystal and the electron wavelength (Tang, 1984), then the crystal can be treated as a pseudo weak phase object (Li & Tang, 1984*a*, *b*). The PPDF of the pseudo weak phase object, $\varphi_{n+1}(x, y)$, would be equivalent to the PPDF of an imaginary isomorph of the crystal, where the real atoms are replaced by the imaginary atoms. The constituent heavy and light atoms of this imaginary isomorph are respectively lighter and heavier than those of the real crystal. Thus the image contrast of the crystal would be roughly proportional to the PPDF of the imaginary isomorph.

The above argument yields the following conclusion. For very thin crystals the image contrast is close to that of WPOA. For thicker crystals, but not thicker than the critical thickness, the image remains closely related to the projection of the crystal structure although it spreads at the positions of atoms. However, the relative contrast of the light atoms is enhanced compared with the heavy atoms. When the crystal is thicker than the critical thickness there is no longer one to one correspondence between the image and the crystal structure.

6. Calculated images of chlorinated copper phthalocyanine

Fig. 5 shows the PPDF of a chlorinated Cu phthalocyanine crystal (Uyeda *et al.*, 1978–79), which is used to check the formula derived. The images calculated for different crystal thicknesses with PWPOA and the multislice method (Cowley & Moodie, 1957) are respectively shown in the left and right columns of Fig. 6. The calculated image in the PWPOA for a one-slice crystal (Fig. 6*a*) is in fact the image in the WPOA. Its contrast is similar to the PPDF (Fig. 5). According to the PWPOA, the images of all atoms become diffuse with the increase of specimen thickness and the contrast of light atoms increases more rapidly than the heavy atoms (Figs. 6*b* and *c*). The centers of the copper atoms begin to turn bright in the image with twelve slices (Fig. 6*d*). This implies that this crystal thickness is thicker than the critical one. The center positions of the chlorine atoms begin to turn bright in the image of 16 slices

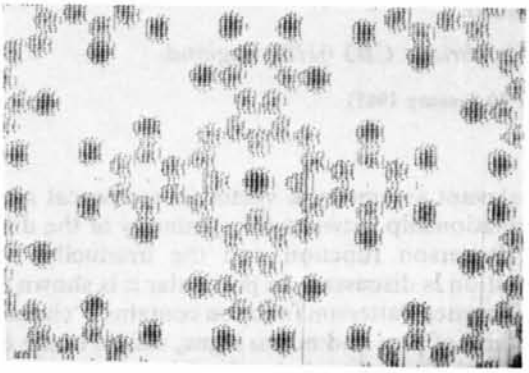

Fig. 5. PPDF of chlorinated Cu phthalocyanine.

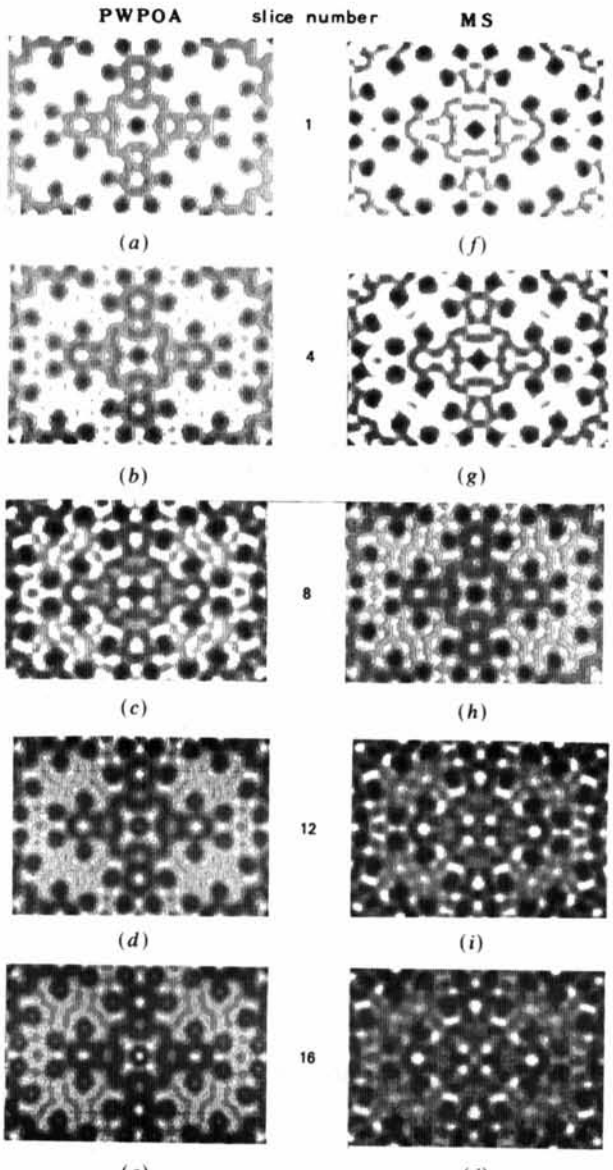

Fig. 6. Calculated images of chlorinated Cu phthalocyanine for different crystal thicknesses and for accelerating voltage 500 kV. (*a*) to (*e*) are calculated with the PWPOA and (*f*) to (*j*) with the multislice method for the spherical aberration coefficient $C_s = 1{\cdot}0$ mm and underfocus 440 Å. The slice thickness is 3.76 Å. The image of a one-slice crystal in PWPOA (*a*) resembles the PPDF (Fig. 5). In the images of four and eight-slice crystals (*b* and *c*) the contrast of light atoms becomes relatively higher. In the image of a 12-slice crystal (*d*) the centers of the copper atoms begin to turn bright. In the image of a 16-slice crystal (*e*) the centers of the chlorine atoms begin to turn bright and copper atoms become brighter, while carbon and nitrogen remain dark. Each corresponding pair of images (*a* and *f*, *b* and *g*, *c* and *h*, *d* and *i*, *e* and *j*) shows a close resemblance at the positions of the atoms but not in the background.

(Fig. 6*e*), where copper atoms become brighter, while carbon and nitrogen atoms remain dark. It can be seen that the corresponding pairs show a close image contrast at the positions of atoms for crystals below the critical thickness (about 56 Å).

7. Validity and advantages of the PWPOA

Since the multislice method in image simulation is widely accepted and usually shows good agreement with the experimental results, it is reasonable to evaluate the limit of the validity of the PWPOA from the comparison of figures in Fig. 6. Obviously, PWPOA can be used to interpret the variation of the image contrast with the crystal thickness at the position of atoms for crystals below the critical thickness. Because in the PWPOA the Fresnel diffraction is taken into consideration while the multiple scattering is neglected, and because the PWPOA can be used for interpreting the image contrast at the positions of atoms but not on the background, we can say that below the critical crystal thickness the deviation of the image contrast from the pure kinematical treatment at the atom positions is mainly caused by the Fresnel diffraction from one slice to the next, while that of the background is by multiple scattering.

Besides, the PWPOA indicates a possibility of revealing preferentially light or heavy atoms in the images for crystals consisting of atoms of different atomic number in the image by choosing different crystal thicknesses. This seems to have more practical meaning for ultra-high-voltage high-resolution electron microscope observation, where the critical crystal thickness allows the crystal being examined to be thicker.

The authors would like to express their gratitude to Professor H. Hashimoto of Osaka University for reading the manuscript and for beneficial discussions. Thanks are also due to his research group for the use of the multislice image simulation program.

References

ALLPRESS, J. G., HEWAT, E. A., MOODIE, A. F. & SANDERS, J. V. (1972). *Acta Cryst.* A**28**, 528-536.
COWLEY, J. M. & IIJIMA, S. (1972), *Z. Naturforsch. Teil A*, **27**, 445-451.
COWLEY, J. M. & IIJIMA, S. (1977). *Phys. Today*, **30**, No. 3, 32-40.
COWLEY, J. M. & MOODIE, A. F. (1957). *Acta Cryst.* **10**, 609-619.
COWLEY, J. M. & MOODIE, A. F. (1960). *Proc. Phys. Soc.* **76**, 378-384.
GRINTON, G. R. & COWLEY, J. M. (1971). *Optik (Stuttgart)*, **34**, 221-233.
ISHIZUKA, K. & IIJIMA, S. (1981). *39th Ann. Proc. EMSA*, pp. 96-97. Baton Rouge: Claitor.
KIRKLAND, E. J., SIEGEL, B. M., UYEDA, N. & FUJIYOSHI, Y. (1980). *Ultramicroscopy*, pp. 479-503.
LI, F. H. & HASHIMOTO, H. (1984). *Acta Cryst.* B**40**, 454-461.
LI, F. H. & TANG, D. (1984*a*). *Acta Phys. Sin. Abstr.* **33**, 1196-1197.
LI, F. H. & TANG, D. (1984*b*). Proc. of the 3rd Asia-Pacific Conference on Electron Microscopy, pp. 60-61.
LYNCH, D. F. & MOODIE, A. F. (1975). *Acta Cryst.* A**31**, 300-307.
SCHERZER, O. (1949). *J. Appl. Phys.* **20**, 20-29.
TANG, D. (1984). Thesis for Master Degree, Institute of Physics, Academia Sinica.
UYEDA, N., KOBAYASHI, T., ISHIZUKA, K. & FUJIYOSHI, Y. (1978-79). *Chem. Scr.* **14**, 47-61.

Acta Cryst. (1985). A**41**, 382-386

The Symmetry Properties of Difference Patterson Functions

BY J. DESMOND C. MCCONNELL

Department of Earth Sciences, Downing Street, Cambridge, CB2 3EQ, England and Schlumberger Cambridge Research, PO Box 153, Cambridge CB2 3BE, England

AND VOLKER HEINE

Cavendish Laboratory, Madingley Road, Cambridge CB3 0HE, England

(*Received* 13 *July* 1984; *accepted* 30 *January* 1985)

Abstract

Difference Patterson functions can be constructed for difference structures arising from superlattice or incommensurate transformations. In each case the difference structure may belong to one of several symmetry types, namely the irreducible representations of the space group of the average structure, at the relevant symmetry **k** vector in reciprocal space. The relationship between the symmetry of the difference Patterson function and the irreducible representation is discussed. In particular it is shown that the difference Patterson function contains a 'character signature' of plus and minus signs, which, in the case of a one-dimensional irreducible representation, identifies that representation uniquely. Examples

0108-7673/85/040382-05$01.50